Towards industrial ultrafast laser microwelding: SiO2 and BK7 to aluminum alloy

Research Article Vol. 56, No. 16 / June 1 2017 / Applied Optics 4873

applied optics

Towards industrial ultrafast laser microwelding: SiO_2 and BK7 to aluminum alloy

Richard M. Carter,[1,*] Michael Troughton,[2] Jianyong Chen,[1] Ian Elder,[2] Robert R. Thomson,[1] M. J. Daniel Esser,[1] Robert A. Lamb,[2] and Duncan P. Hand[1]

[1]Institute of Photonics and Quantum Sciences, Heriot-Watt University, Edinburgh, EH14 4AS, UK
[2]Leonardo MW Ltd., 2 Crewe Road North, Edinburgh, EH5 2XS, UK
*Corresponding author: r.m.carter@hw.ac.uk

Received 1 March 2017; revised 7 May 2017; accepted 9 May 2017; posted 9 May 2017 (Doc. ID 287698); published 1 June 2017

We report systematic analysis and comparison of ps-laser microwelding of industry relevant Al6082 parts to SiO_2 and BK7. Parameter mapping of pulse energy and focal depth on the weld strength is presented. The welding process was found to be strongly dependent on the focal plane but has a large tolerance to variation in pulse energy. Accelerated lifetime tests by thermal cycling from −50° to +90°C are presented. Welds in Al6082-BK7 parts survive over the full temperature range where the ratio of thermal expansion coefficients is 3.4:1. Welds in Al6082-SiO_2 parts (ratio 47.1:1) survive only a limited temperature range.

OCIS codes: (140.0140) Lasers and laser optics; (320.0320) Ultrafast optics; (140.3390) Laser materials processing; (320.5390) Picosecond phenomena; (320.7160) Ultrafast technology; (220.4610) Optical fabrication.
https://doi.org/10.1364/AO.56.004873

1. INTRODUCTION

Ultrafast laser microwelding has been the subject of significant sustained development in recent years. The combination of high precision, high speed, and low thermal damage while removing the necessity for an interlayer presents a unique solution to the problems of bonding highly dissimilar materials [1–9].

In dissimilar material bonding, where only one material is transparent to the incident radiation, the advantage of an ultrafast laser lies in the combination of severely restricted thermal zones and the ability to trigger both nonlinear absorption in the transparent material and linear absorption in the opaque material. This generates a small heated zone around the interface forming of plasma in both materials simultaneously. As the plasma mixes and cools, a true weld is formed [5,9].

While it is possible to form such bonds using a high-power, single-shot laser system [9], fast and effective welding is generally dependent on thermal accumulation from multiple pulses. This is particularly true where non-ideal mating at the interface results in a micro-gap. Through thermal accumulation, a small melt volume can be produced around the weld that flows into and fills the gap ahead of the welding process. This requires a minimum repetition rate for the laser system such that the energy from the previous pulse has not dissipated by the time the next pulse arrives. While this is naturally material dependent, this dissipation is generally on the order of milliseconds, and therefore the required repetition rate is on the order of hundreds of kHz.

The majority of research on ultrafast laser micro-welding has focused on similar or slightly dissimilar material bonding (i.e., glass–glass) with either a fs laser [5,7,9–15], or, more recently, ps pulses [16–19]. However, there is limited published data on the bonding of highly dissimilar materials. The bulk of the work in this area has concentrated on bonding of glass–silicon with both fs [14,20] and ps systems [21–23]. For glass–metal bonding, publications have been limited to proof-of-principle demonstrations [24–27] using fs systems involving specific material combinations and limited systematic study.

In this paper, we aim to move ultrafast microwelding closer to an industrially viable technique through a systematic study of the parameter space for welding and demonstrating accelerated lifetime survivability.

2. MATERIALS

Spectrosil 2000 (SiO_2), Schott N-BK7 (BK7), and Al6082 were chosen as materials of interest for this study. These are typical materials used for a range of industrial applications, and care was taken to make the tests as representative of an industrial process as possible. SiO_2 and BK7 were sourced in the form of 10 mm (±0.2 mm) cubes. These cubes have two sets of parallel polished faces (optical, $\lambda/4$, flatness). This specification was deemed sufficient to demonstrate the

Table 1. Comparison of the Ambient Thermal Properties of the Materials Used Within this Study

Material	Melting/ Softening Point (°C)	Thermal Conductivity (W m^{-1} K^{-1})	Linear Thermal Expansion (10^{-6} K^{-1})
Spec.2000 [29]	1600	1.38	0.51
N-BK7 [30]	719	1.114	7.1
Al6082 [31]	555	180	24

capacity to weld "bulk" optical components. A 0.2 mm tolerance of the cubes was deemed adequate given the comparatively long Rayleigh length of the focal optics (see Section 3 below). In practice, the tolerance of the delivered parts is significantly better than 0.2 mm, closer to 0.02 mm.

Al6082 was sourced in the form of 15 × 15 × 5 ± 0.2 mm metal coupons in T6 temper condition. One 15 × 15 face has been further processed by grinding to a specified Ra of 0.3–0.4 μm. This was confirmed with an Alicona 4G surface profiler and found to have an average Ra of 288 nm. This is rougher than the polished surfaces used for our previous projects on glass–metal bonding [28] (with an Ra <100 nm) and is optically rough. It was initially anticipated that a processing step may be necessary to reduce the surface roughness before laser welding; however, this was found not to be required.

Before bonding, all materials were cleaned thoroughly. BK7 and SiO_2 parts were washed in acetone then wiped using lint-free lens tissue with the drag-and-drop technique on one face (the bonding contact face). This was followed by washes with acetone, isopropan–2–ol, and methanol before being dried with ionised nitrogen. The bonding contact face was visually inspected for dirt, residue, or solvent before being placed in contact.

The Al6082 parts were cleaned in acetone with an ultrasonic bath for 5 mins before being wiped clean with lint-free lens tissue. This was followed by a further 5 mins ultrasonic bath in acetone, and, finally, the same cleaning process as was used for the glass was applied to the parts before use. Note that in this case only the ground Al surface required complete cleaning.

A table of the comparative ambient thermal properties is presented below for reference (Table 1). Of particular interest are the differences in the coefficients of thermal expansion, which will affect thermal cycling lifetime tests.

3. EXPERIMENTAL PROCEDURE

Due to the brittle nature of glass, a full, statistically relevant test would require at least 20 samples for each set of laser welding process parameters. This rapidly becomes impractical unless a limit is placed on the variables under test. For the tests in this study, scan speed, repetition rate, numerical aperture, and pulse duration have all been kept constant, while pulse energy (average power) and focal plane have been varied.

Even with only two test parameters, a full parameter map would require in excess of 1000 individual welds. As this many tests is impractical in terms of cost and time, two separate tests were performed. First, a parameter map was made by carrying out two individual tests for each pair of parameters (pulse energy and focal plane). From these two tests, the parameter pair was labeled. If both tests failed to weld, the parameters were labeled as "failed." If both parts welded and remained welded over a period of 24 h, the parameters were labeled as "welded." Finally, if either part had failed in less than 24 h or if only one part was welded, the parameters were labeled as "partial."

It should be noted that these tests can inform us only of the general shape of the available parameter space for welding, since two tests are not fully representative. From this parameter map, regions of interest were selected for a full, 20-sample test using shear strength as a metric for the quality of the bond. From these tests, an "optimized" set of parameters was identified and these subjected to accelerated lifetime testing, e.g., thermal cycling, to determine the applicability of laser microwelding for industrial applications.

A. Welding Setup

The experimental procedure is similar to our previously reported system [28], Fig. 1, with an alteration to the clamping system, Fig. 2. Experiments were performed either with this setup or, in later tests, with improvements to the collimation of the telescoping system, and hence an improved (smaller) focal spot as well as stage movement, described below. In all cases, experiments were carried out using a Trumpf TruMicro 5 × 50 laser emitting 5.9 ps, 1030 nm pulses with a repetition rate of 400 kHz. Although the system does allow for pulse picking to generate lower repetition rates, the next available repetition rate is 200 kHz, which is insufficient for thermal accumulation and hence was not investigated. Fig. 1 shows a schematic of the laser setup. In this case, the focusing optic is a 20 mm (Thorlabs LA1074) plano-convex AR coated for 600–1050 nm, creating a theoretical focal spot in air of 3.4 μm (NA 0.25). This optic was chosen to allow for thicker, more representative glass pieces (up to ∼26 mm) in comparison to our earlier studies [28].

As a fixed optic is used, translation stages are employed to scan samples through the laser focus. Our early experiments used Areotech pro115 screw stages; however, these exhibit significant backlash, and the accuracy is limited to ∼6 μm. For the improved system, we incorporated a sub-stage assembly consisting of ANT95-50XY-MP PLUS Aerotech nano-positioning stages with an accuracy of ±250 nm. Note that due to the improvement in the translation accuracy and backlash, it is not appropriate to directly compare results from the two sets of stages.

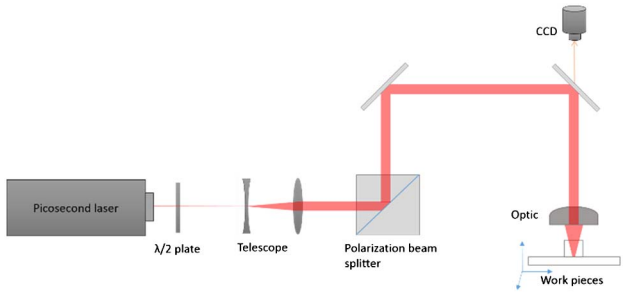

Fig. 1. Schematic of laser welding system. The polarizing beam splitter provides the capability for fine adjustment of the incident pulse energy. Note that for these experiments, a clamp arrangement was used to hold the work pieces together, as outlined in Fig. 2.

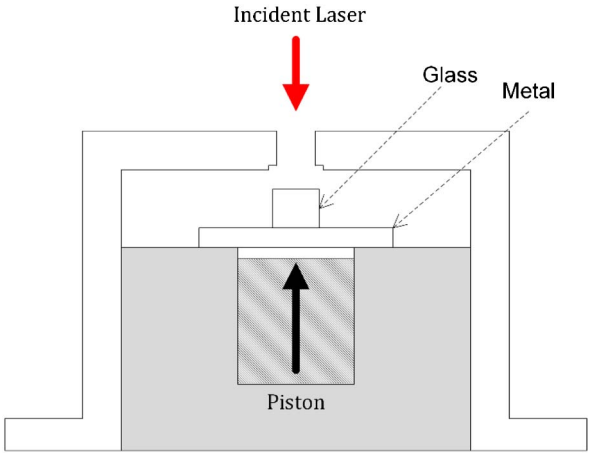

Fig. 2. Schematic of the pneumatic clamp system, here a 10 mm BK7 cube is clamped to a 15 × 15 × 5 mm Al6082 test piece.

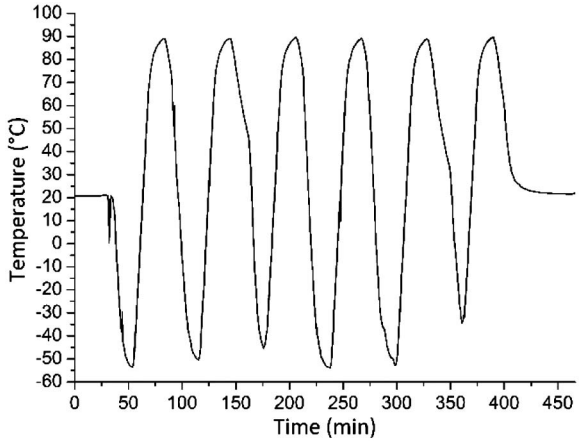

Fig. 3. Example of the thermal cycling regime.

The chosen weld pattern is an inward-moving arithmetic spiral. This pattern allows a single continuous weld seam to be drawn with no corners to accumulate stress [28]. In all cases, the pattern has a pitch of 0.156 mm, a starting radius of 1.25 mm, and a final radius of 0.156 mm and was translated at 0.8 mm s^{-1}.

In order to control the focal plane to the accuracy demanded by the welding application, a charged-coupled device (CCD) array was employed imaging through the back of a partially polished mirror. At low power, the Fresnel reflections from the various surfaces can be separately resolved and re-focused onto the CCD through the focusing optic. Since the CCD has no lens of its own, this focal position is offset from the true focus of the surface by a constant displacement (determined separately) dependent on the optic and collimation of the incident beam. For glass–metal welding, this process is used to identify the upper (glass-air interface) to within ±10 μm. Given the dimensions of the glass cube, this surface is a known distance from the metal/glass interface (10 mm ± 0.2 mm, with suitable compensation for the material refractive index). Due to the scattering surface of the metal, this interface is hard to identify directly. Note that the convention used here is that $z = 0$ is the glass–metal interface with negative foci being under the metal surface (in reality, the beam is defocused onto the metal surface [32]).

One of the key challenges in ultrafast microwelding is ensuring that the two materials are close enough to prevent plasma escaping from the focal volume. This generally requires optical contact or close to optical contact separation of the two work pieces. While this is readily achievable for optical (glass) surfaces, it is more challenging for metal surfaces, which generally require some pre-processing and force to push the two surfaces into contact. Figure 2 shows the pneumatic clamp used to ensure close contact. This system is modified from our previously reported clamping method [28] and is similar to those reported in the literature (e.g., [5,6,9,13]).

B. Shear Tests

In order to provide a metric for the strength/quality of bonds, shear tests were carried out using the technique previously reported in Ref. [28]. Note that in this case, the failure mechanism(s) of the components appears complex, and in most cases seems to be the result of more than one mechanism. As a consequence, no attempt has been made to fit a Weibull modulus to the results.

C. Thermal Cycling

Although ultrafast laser microwelding allows the joining of highly dissimilar materials, this is accomplished by strictly limiting the thermal zone to a few hundred micrometers around the focus of the laser, hence effectively keeping the bulk material at room temperature (~25°C). It is therefore to be expected that post welding thermal cycling will be a significant issue due to the large mismatch in thermal properties (cf. Table 1).

As thermal cycling is generally a requirement for industrial applications, tests were carried out within a thermal chamber cycling from +90° to −50°C at a rate of 1°C min^{-1} for 6 cycles, a measurement of which is shown in Fig. 3.

Micrographs of samples tested were recorded before and after thermal cycling applying a 20N shear force to determine if the bonds retain sufficient strength for industrial uses.

4. RESULTS AND DISCUSSION

It was found that standard single-pass welding was unable to provide a suitably robust, reliable welding process when welding SiO_2 to unpolished metals (including our representative Al6082). Consequently, a double-pass welding process was developed for this material combination. The second pass follows the first with a delay of 3 s but is otherwise identical in terms of incident energy, scan speed, focal depth, etc. (Note that this is the delay between the end of the first pass and the start of the second. As the full spiral requires 40 s, including stage movement time, the second pass is therefore 43 s behind the first over the same area.) It is worth noting that the introduction of a second pass significantly increases the available parameter space for laser welding, further complicating process optimization. It is notable that the nano-positioning piezo stages were required for this process to work—i.e., it is necessary that the second pass precisely repeats the path of the first pass.

We hypothesize that glass melt is required to fill any incidental (<1 μm) gaps between the glass and the metal before the

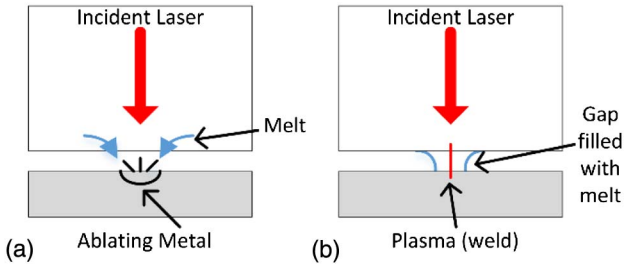

Fig. 4. Illustration of the double-pass welding technique. (a) First pass and (b) second pass.

plasma can weld the two materials together. In the case of BK7, its low melting point ensures that there is sufficient physical separation between the edge of the heat-affected zone (melt) in the glass and the plasma induced by absorption such that a bow wave of melt can fill the gap ahead of the plasma. In the case of SiO_2, this is not observed. The first pass of the laser will succeed only in melting the glass onto the metal, with no welding taking place. The second pass is then required to bond the materials using the now well-confined plasma (Fig. 4).

Further experimentation and direct measurement of the melt flow and plasma dynamics are underway to confirm this [33].

A. Parameter Mapping

Figure 5 shows the results of the parameter mapping. In this case, all results presented are for the improved welding rig for consistency. In most cases, only two samples were tested for each parameter pair and as a result cannot be regarded as entirely representative.

Of interest here is the apparently large range of average powers over which laser microwelding is possible, from 3.5 to 6.5 W in BK7 (average powers above this level were found, qualitatively, to be less reliable) and 4.5–9 W with SiO_2. By comparison, the available focal range is limited to ~200 μm in both materials and clearly indicates that, for these focal conditions, defocus on the surface of the metal is required. This may imply that an arrangement providing a slightly larger spot size on the metal surface may be more appropriate, although the absorption dynamics require balancing of nonlinear processes in the glass and linear processes on the metal surface, which may not scale in an easily predictable fashion.

B. Focal Plane

To investigate more closely the effect of the focal plane on the resulting weld, a nominal 6.55 W was chosen and a statistically relevant number (>20) of samples prepared and subjected to shear test. To reduce the number of tests required, only Al6082-BK7 was systematically tested; however, the qualitative results for SiO_2 agree with the observed trend. This test was carried out using the slightly expanded spot from the original telescoping system setup, and as such, a slightly higher average power was used to compensate for the increased focal spot size (6.55 W was found to provide equivalent results to 5 W with optimized telescoping). The results are, however, still representative of the relationship among focal positions for a given average power and provide an interesting insight into the effect of errors in the optical system.

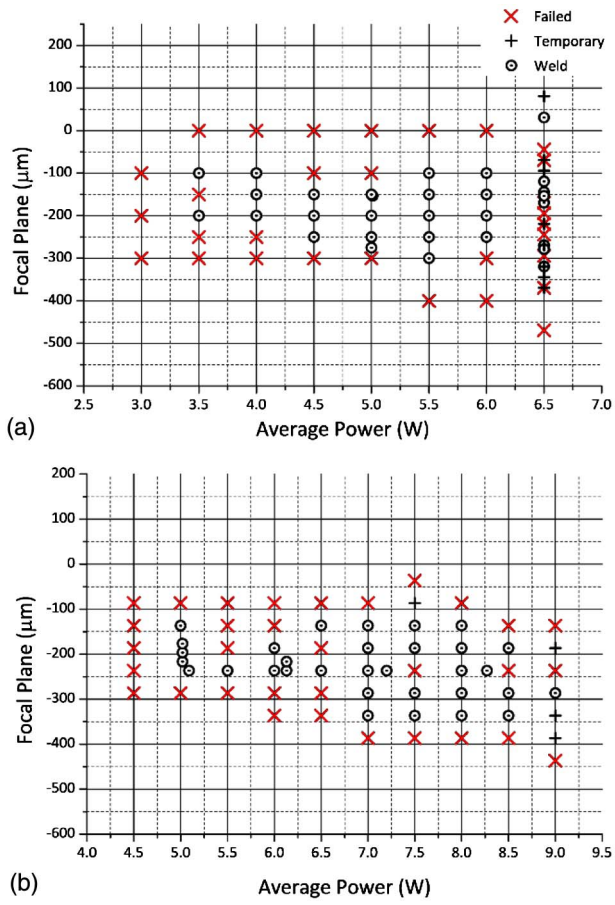

Fig. 5. Parameter map of (a) Al6082-BK7 and (b) Al6082-SiO_2 welding with 400 kHz, 6 ps pulses translated at 0.8 mm s^{-1}.

Three separate focal planes, covering the range of available parameters, were chosen at −231, −131, and −31 μm. Figure 6 shows the results of these shear tests where $P_s(V_o)$ represents the probability of surviving the applied parameter (in this case, strain) [28].

The results clearly indicate the presence of an optimal weld parameter around −131 μm with a significant drop in both the

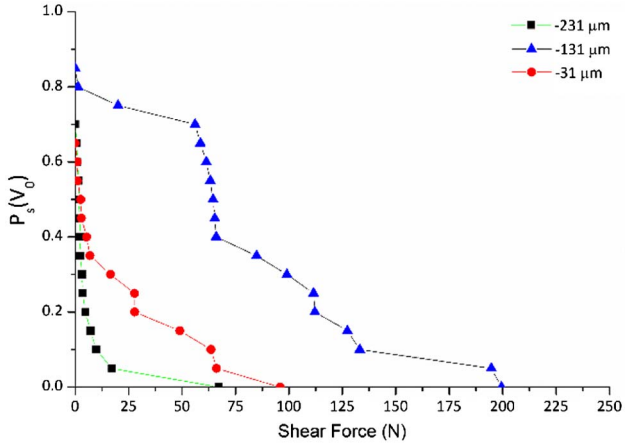

Fig. 6. Weibull shear test results for varying focal plane at a constant 6.55 W average power for Al6082-BK7 welding.

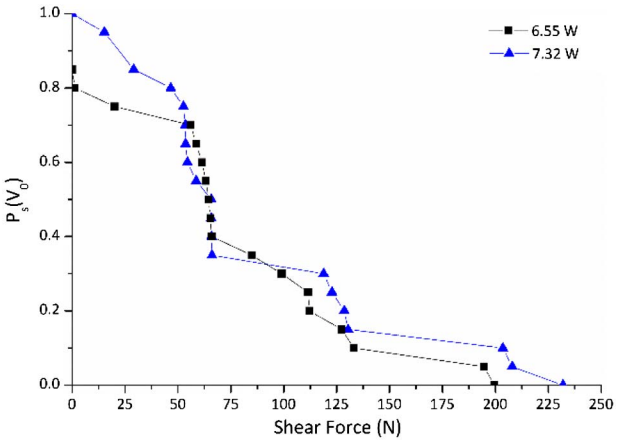

Fig. 7. Weibull shear test results for varying incident power with a constant focal plane of −131 μm for Al6082-BK7 welding.

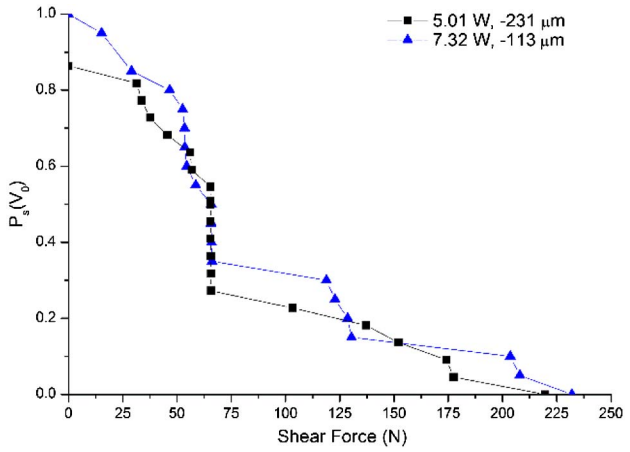

Fig. 8. Weibull shear test results for best parameters at 5 W, −153 μm for Al6082-BK7 welding. Equivalent results were obtained at 7.32 W and −113 μm with the larger spot size produced with the original telescoping system and have been plotted here for comparison.

weld strength and reliability from a movement in focus of 60 μm in either direction. This demonstrates that considerable care is required to ensure the focal plane is accurately positioned in order to maintain repeatability in weld strength (cf. the nominal tolerance of ±200 μm on the thickness of the glass cubes).

C. Incident Power

With the correct focal range identified, an additional test was performed to determine the effect of increasing the average power. Again the results are presented for the slightly increased spot size telescope arrangement in BK7. As mentioned above, a slight increase in average power is necessary to maintain weld reliability in comparison to the optimized telescope (cf. optimal parameters in Section 4.D below), in this case, from 6.55 to 7.32 W. The results of this test are presented in Fig. 7, where we can see that the strength of the weld has not been significantly altered as a result of changing the incident power. This, combined with the large range of useable average powers from the parameter mapping, demonstrates that there is a large tolerance in average power for the welding process.

D. Best Parameters

To date the best parameters for Al6082-BK7 welding have been observed at 5 W, −153.3 μm with the improved telescoping system. The result of the shear test for these parameters is presented in Fig. 8 and is similar in terms of reliability and optimal strength to those presented in Fig. 7 (reproduced in Fig. 8 for clarity). The effect of adjusting the spot size (i.e., telescope) has been to decrease the required average power (pulse energy) as expected (cf. Section 3.A), but also to move the optimal focal position by 20 μm into the metal surface. This suggests that the ratio of energy densities between the glass and the metal surface are critical.

These parameters provide a yield at 0 N of 0.86 and a 60 N yield of 0.64. Further optimization would likely increase the yield at 60 N, while more precise components and a clean room would likely increase the yield at 0 N.

The best parameters for Al6082-SiO_2 welding have been observed at 6.13 W −236.7 μm. The shear tests, Fig. 9, of these parameters gives a yield of 0.79 at 0 N and 0.54 at 60 N. Further optimization is possible for this material combination (particularly as the double-pass welding has several more degrees of freedom to investigate).

E. Weld Failure Examination in BK7

The absolute failure of the welds may be misleading, as stress-induced cracks appear before the weld entirely fails. Figure 10 shows the result of a typical shear test. Observations show that the form of this load graph is reproducible among samples and even among different glasses. The chief difference among tests is where on the curve failure occurs. The load associated with the plateau is consistent (to within 3 N) for all BK7 samples that exhibited enough strength to reach it; however, the length of the plateau (in terms of strain) is not consistent.

The form of the strength test in Fig. 10 does not correspond to standard results for either brittle or ductile materials. In particular the level plateau region is difficult to explain. In order to rule out a systematic error on the part of the test rig, two additional Al6082-BK7 parts were created with the intention of halting the break test at various stages of the curve. The first

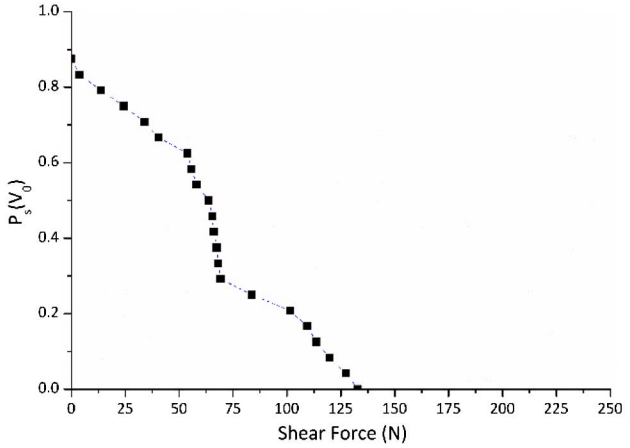

Fig. 9. Weibull shear test results for best parameters: 6.13 W, −236.7 μm for Al6082-SiO_2 welding.

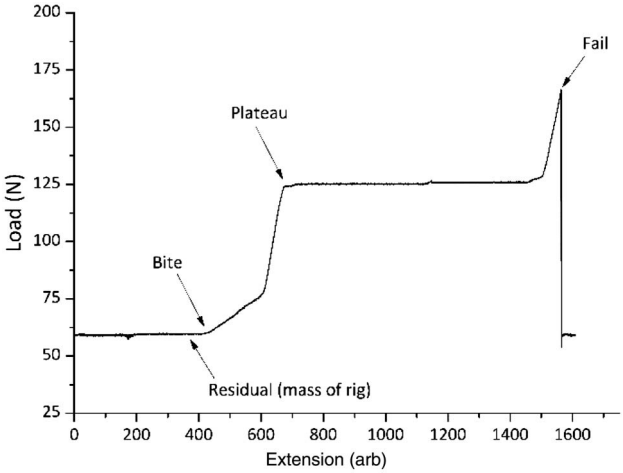

Fig. 10. Example plot of measured force versus extension during shear test for a Al6082-BK7 part.

part was halted at the start of the plateau, and the second part halted approximately half way through the plateau. Both parts survived the test and remained bonded.

Figure 11 shows micrograph images of the two parts halted during the break test. From this result (and from examining the remaining broken parts from previous tests), it is clear that the plateau region indicates that a crack forms and then propagates around the weld region. From the failed parts, it seems that this crack is not responsible for the final fail of the weld. The crack occurs at or near the interface but rather propagates into the bulk glass and self-terminates (once the stress in the bulk glass has been sufficiently relieved).

A similar weld failure mechanism can also be seen in the SiO_2 bonding process, Fig. 9; however, the effect is less pronounced and it was not possible to observe crack propagation as reliably in these components.

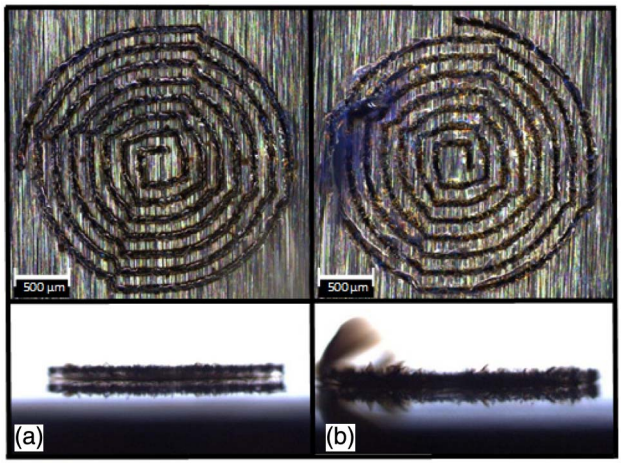

Fig. 11. Microscope images of partly tested examples. (a) Part stopped at start of plateau region and (b) part stopped in plateau region. A crack is clearly visible in the right example. Lower images are transmission micrographs taken normal to the weld plane (note the weld region in the metal is not observable, and the weld in the glass has been reflected from the interface). The backlash due to the use of screw stages is clear from the non-perfect spiral in the images.

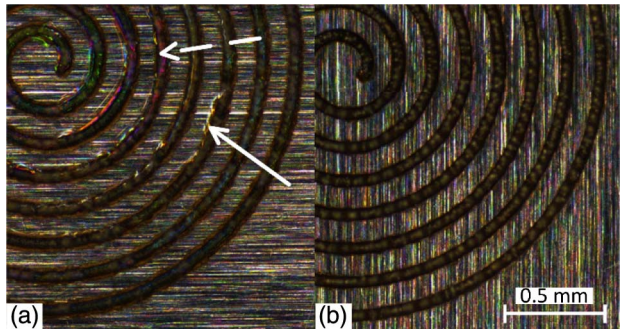

Fig. 12. Example micrographs of Al6082-SiO_2: (a) poor weld with delamination (colored interference within the welds, dashed arrow) and macro cracking (between welds—solid arrow), and (b) a good weld.

F. Weld Diagnostics in SiO_2

As part of the effort to improve the welding process, an attempt has been made to identify poor welds. It is possible to diagnose poor welds for this material combination by observing the weld under a microscope. Figure 12 illustrates this principle. The appearance of significant macro-scale cracks and/or delamination of the weld structure indicates a weak weld. Although there are no clear means to identify the absolute strength of the bond from the micrographs, and in particular the very strong bonds, this provides a mechanism for quality control of laser microwelded parts by eliminating very poor bonds. Note that this is more practical than BK7, due to the absence of microcracking observed in Al6082-BK7 welding.

G. Thermal Cycling, Al6082-BK7

Twelve Al6082-BK7 parts were generated using the slightly increased spot size telescope arrangement at 7.32 W at a focus of −131 µm for thermal cycling. These parameters correspond to optimal weld strength for this focal setup. These are indexed 8.2.1–8.2.12 (see Table 2 and Figs. 13 and 14). Of these, two failed during welding (8.2.8 and 8.2.12) and one other (8.2.1) failed after welding, which is consistent with the weld fail probabilities indicated in Fig. 8. Micrographs of each were recorded with observations both before (Fig. 13) and after (Fig. 14) the thermal tests.

Table 2. Observations and Results of Thermal Cycling Tests for 12 Optimized Al6082-BK7 Parts

Part #	Observations	Thermal Cycling	20 N Shear
8.2.1	Weld failed under minimal handling	NA	NA
8.2.2	Normal	Pass	Pass
8.2.3	Normal	Pass	Fail at 19.9 N
8.2.4	Normal	Pass	Pass
8.2.5	Normal	Pass	Fail at 16 N
8.2.6	Normal	Pass	Pass
8.2.7	Smooth appearance; indicative of poor weld	Fail	NA
8.2.8	Weld failed	NA	NA
8.2.9	Normal	Pass	Pass
8.2.10	Normal	Pass	Pass
8.2.11	Slight delamination; indicative of weaker weld	Fail	NA
8.2.12	Weld failed	NA	NA

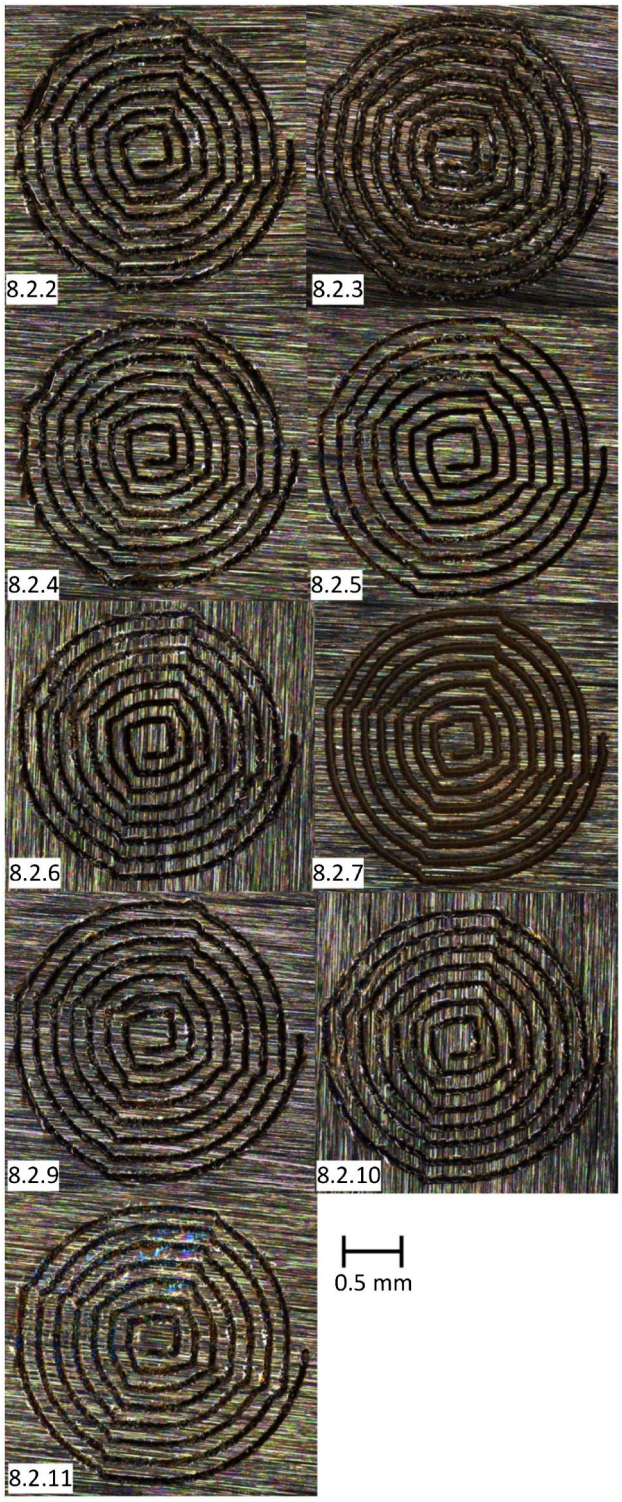

Fig. 13. Microscope images of Al6082-BK7 parts before thermal cycling.

Note that minor cracking of the surface is indicative of a good weld. Although somewhat counter-intuitive, minor cracks around the melt volume (particularly in the glass) are to be expected given the significant difference in the thermal expansion coefficients in the two materials (Table 1). As the weld cools, thermal stress is relieved through small cracks forming in the glass around the melt as shown in Fig. 14. However, this does not indicate a reduction in the weld strength.

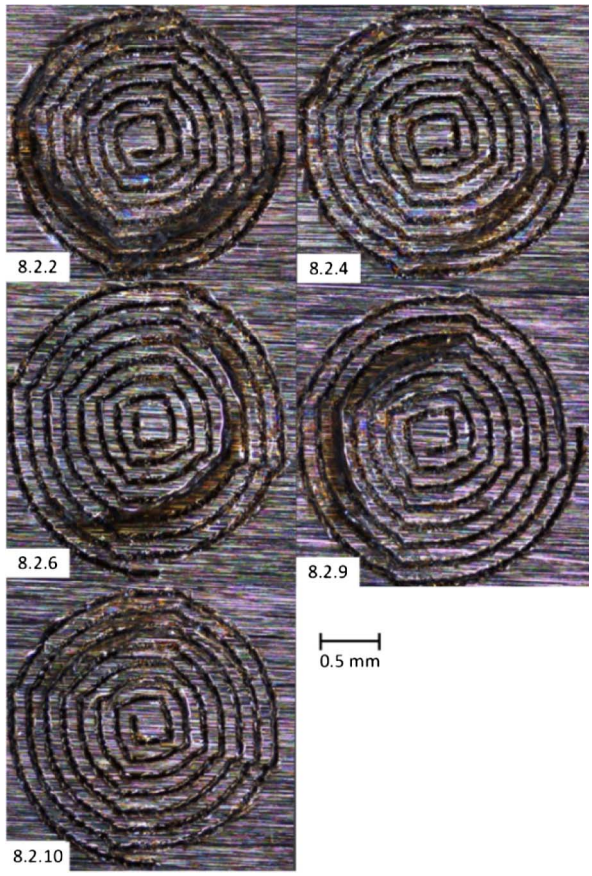

Fig. 14. Microscope images of surviving Al6082-BK7 thermally cycled and 20 N shear tested parts.

In comparing the images of the welds before thermal cycling (Fig. 13) and after (Fig. 14) images of the welds, it is clear that the thermal cycling process introduced considerable strain into the glass–metal welds and macro-scale cracks have formed to release some of the stress. Although these large cracks have potentially reduced the strength of the bonds after thermal cycling, the strength is still sufficient for the vast majority of applications, as can be seen in Table 2.

Table 3. Observations and Results of Thermal Cycling Tests for 12 Optimized Al6082-SiO_2 Parts

Part	Observations	Thermal
13.2.1	Weld Failed	NA
13.2.2	Normal	Fail
13.2.3	Weld Failed	NA
13.2.4	Micro cracks	Fail
13.2.5	Normal	Fail
13.2.6	Normal	Fail
13.2.7	Delaminated and cracked centre	Fail
13.2.8	Small crack to one side	Fail
13.2.9	Normal	Fail
13.2.10	Small crack to one side	Fail
13.2.11	Small crack to one side	Fail
13.2.12	Normal	Fail

H. Thermal Cycling, Al6082-SiO_2

Twelve parts were generated using the larger spot size telescope arrangement at 6.13 W at a focus of −236.7 μm for thermal cycling. These parameters correspond to optimal weld strength for this focal setup. These are indexed 13.2.1–13.2.12 (see Table 3 and Fig. 15). Of these, two failed during welding (13.2.1 and 13.2.3), which is consistent with the weld fail probabilities indicated in Fig. 9. Micrographs of each were recorded with observations before (Fig. 15) the thermal tests.

None of the parts survived thermal cycling. Although this is not unexpected given the significant thermal mismatch in the expansion coefficient between the two materials (×47.1), it stands in contrast to the BK7 (expansion miss-match of ×3.4), indicating that although bonds can be formed through microwelding, a significant mismatch in material properties will result in poor lifetime performance.

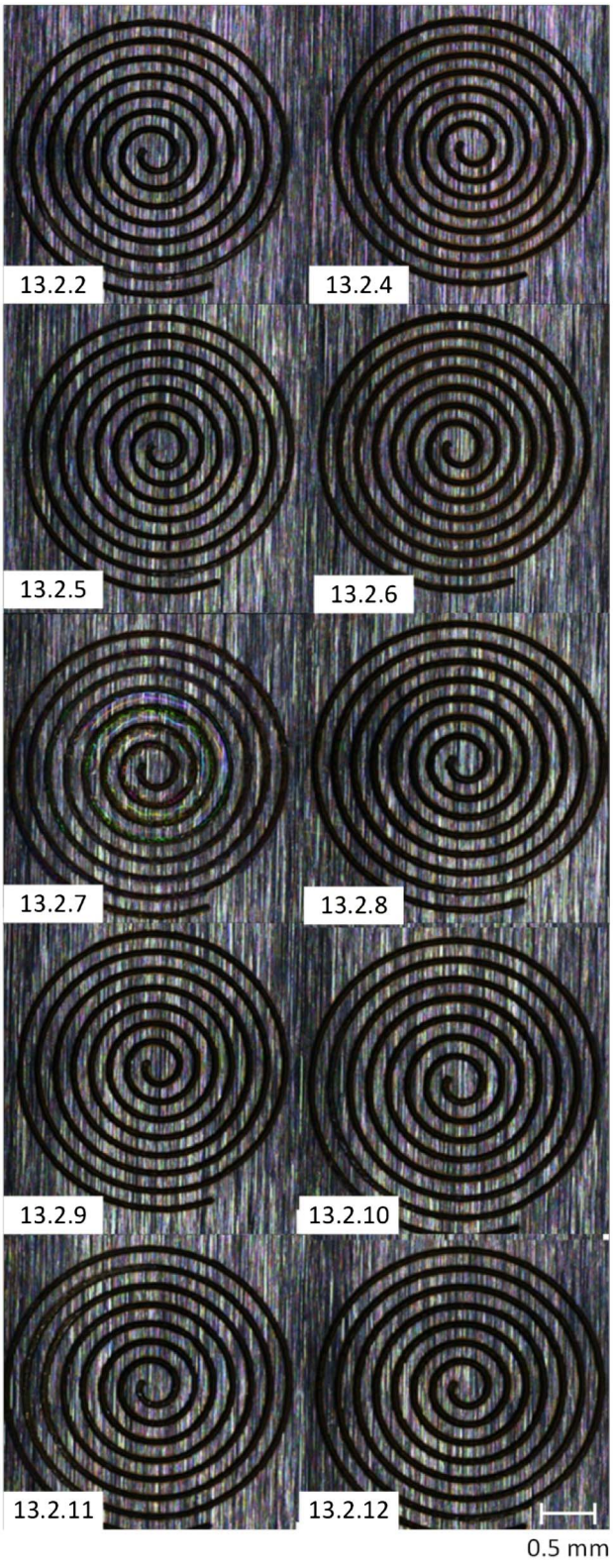

Fig. 15. Microscope images Al6082-SiO_2 test parts before thermal cycling.

5. CONCLUSIONS

The process analysis presented here represents the first of many steps towards a reliable and robust laser process. Further work will be necessary to investigate process scaling and process speed and to improve on the <80% process yield that has been thus far demonstrated. The results presented above demonstrate some of the difficulties and strengths inherent in moving a novel laser process from proof of principle to a repeatable and standardized process. The combination of results for the parameter mapping, power variation, and focal depth demonstrates the need for detailed analysis of potential processing parameters.

The results presented for Al6082–BK7 welding demonstrate that a robust, reliable, and simple welding process is achievable. The mean strength of these bonds, in the region of 13 MPa (assuming a 2.5 mm diameter bond), compares well with the proof-of-principle demonstrations published elsewhere using fs laser pulses [25–27] but, crucially, does not require polished metal surfaces in our case. The demonstrated thermal cycling survivability and the strength of the bonds are both well within the range of interest for the majority of optic–metal bonding applications. While the process yield requires further work to increase beyond 80%, there is clearly significant potential in areas where adhesive bonding presents issues due to creep, outgassing, and thermal management issues.

Given that SiO_2 to Al welding has previously been demonstrated using polished metal surfaces [28] the failure of a single-pass process to weld SiO_2 to Al6082 is likely due to the roughness of the Al surface. This roughness generates a local gap between the two surfaces. However, this roughness is clearly much less of an issue with BK7 to Al6082 welding, which is readily achievable with a single pass. It is postulated that the roughness of the surface must combine with material properties of SiO_2, namely, the higher melting temperature and lower thermal expansion. This will result in a lower volume of glass melt in the weld. This has been demonstrated to be critical in bridging gaps in glass–glass welding [32], and, since analysis of the weld structure indicates a much smaller metal melt volume [33], it is reasonable to suppose the glass melt volume is also instrumental in bridging gaps in metal–glass welding. By use of a double-pass welding process, this limitation can be overcome, suggesting that multi-pass welding offers the potential to deal with rougher surfaces or standoffs for metal–glass welding in general.

Although further optimization of welding parameters is likely to result in stronger and more reliable bonding, it is unlikely to be able to compensate for the high mismatch in thermal expansion. Further work in thermal compensation, either through interlayers or surface patterning to relieve thermal stress, will therefore be required before a reliable process can be developed, particularly for material combinations with a large mismatch of thermal expansion, e.g., Al6082-SiO_2.

It is, however, notable that despite a different weld mechanism being required for reliable SiO_2 to Al6082 bonding compared with BK7 to Al6082, the optimal weld parameters in each case are very similar and easily within the capabilities of one laser system. Indeed, the parameter mapping presented above suggests a large tolerance to laser pulse energy (average power); the results of the weld process are much more dependent on the focal system (i.e., ± 100 μm in the focal plane). This, combined with previous proof-of-principle demonstrations in a wide range of materials [28], illustrates the enormous flexibility and potential for a single-laser system to weld a large range of materials given suitable beam delivery optics and sufficient optimization of the precise parameters.

Funding. Engineering and Physical Sciences Research Council (EPSRC) (EP/K030884/1); Science and Technology Facilities Council (STFC) (ST/H005595/1).

Acknowledgment. M. J. Daniel Esser would like to acknowledge the financial support received from the Royal Academy of Engineering and Leonardo MW Ltd. for the Research Chair in Laser Device Physics & Engineering.

REFERENCES

1. F. Niklaus, G. Stemme, J.-Q. Lu, and R. J. Gutmann, "Adhesive wafer bonding," J. Appl. Phys. **99**, 031101 (2006).
2. J. Oberhammer, F. Niklaus, and G. Stemme, "Sealing of adhesive bonded devices on wafer level," Sens. Actuators A **110**, 407–412 (2004).
3. A. W. Y. Tan and F. E. H. Tay, "Localized laser assisted eutectic bonding of quartz and silicon by Nd:YAG pulsed-laser," Sens. Actuators A, Phys. **120**, 550–561 (2005).
4. Q. Wu, N. Lorenz, and D. Hand, "Localised laser joining of glass to silicon with BCB intermediate layer," Microsyst. Technol. **15**, 1051–1057 (2009).
5. H. Huang, L.-M. Yang, and J. Liu, "Ultrashort pulsed fiber laser welding and sealing of transparent materials," Appl. Opt. **51**, 2979–2986 (2012).
6. S. Richter, S. Döring, F. Zimmermann, L. Lescieux, R. Eberhardt, S. Nolte, and A. Tünnermann, "Welding of transparent materials with ultrashort laser pulses," Proc. SPIE **8244**, 824402 (2012).
7. W. Watanabe, S. Onda, T. Tamaki, K. Itoh, and J. Nishii, "Space-selective laser joining of dissimilar transparent materials using femtosecond laser pulses," Appl. Phys. Lett. **89**, 021106 (2006).
8. W. Watanabe, T. Tamaki, and K. Itoh, "Ultrashort laser welding and joining," in *Femtosecond Laser Micromachining*, O. Roberto, C. Giulio, and R. Roberta, eds. (Springer-Verlag, 2012), pp. 467–477.
9. P. Kongsuwan, G. Satoh, and Y. L. Yao, "Transmission welding of glass by femtosecond laser: mechanism and fracture strength," J. Manuf. Sci. Eng. **134**, 011004 (2012).
10. T. Tamaki, W. Watanabe, and K. Itoh, "Laser micro-welding of transparent materials by a localized heat accumulation effect using a femtosecond fiber laser at 1558 nm," Opt. Express **14**, 10460–10468 (2006).
11. D. Hélie, M. Bégin, F. Lacroix, and R. Vallée, "Reinforced direct bonding of optical materials by femtosecond laser welding," Appl. Opt. **51**, 2098–2106 (2012).
12. T. Tamaki, W. Watanabe, J. Nishii, and K. Itoh, "Welding of transparent materials using femtosecond laser pulses," Jpn. J. Appl. Phys. **44**, L687–L689 (2005).
13. A. Horn, I. Mingareev, A. Werth, M. Kachel, and U. Brenk, "Investigations on ultrafast welding of glass-glass and glass-silicon," Appl. Phys. A **93**, 171–175 (2008).
14. S. Richter, S. Döring, A. Tünnermann, and S. Nolte, "Bonding of glass with femtosecond laser pulses at high repetition rates," Appl. Phys. A **103**, 257–261 (2011).
15. K. Sugioka, M. Iida, H. Takai, and K. Micorikawa, "Efficient microwelding of glass substrates by ultrafast laser irradiation using a double-pulse train," Opt. Lett. **36**, 2734–2736 (2011).
16. I. Miyamoto, A. Horn, and J. Gottmann, "Local melting of glass material and its application to direct fusion welding by ps-laser pulses," J. Laser Micro/Nanoeng. **2**, 7–14 (2007).
17. I. Alexeev, K. Cvecek, C. Schmidt, I. Miyamoto, T. Frick, and M. Schmidt, "Characterization of shear strength and bonding energy of laser produced welding seams in glass," J. Laser Micro/Nanoeng. **7**, 279–283 (2012).
18. I. Miyamoto, K. Cvecek, Y. Okamoto, and M. Schmidt, "Novel fusion welding technology of glass using ultrashort pulse lasers," Phys. Procedia **5**, 483–493 (2010).
19. I. Miyamoto, K. Cvecek, and M. Schmidt, "Evaluation of nonlinear absorptivity in internal modification of bulk glass by ultrashort laser pulses," Opt. Express **19**, 10714–10727 (2011).
20. A. Horn, I. Mingaeev, A. Werth, and M. Kachel, "Joining of thin glass with semiconductors by ultra-fast high-repetition laser welding," Proc. SPIE **6880**, 68800A (2008).
21. I. Miyamoto, Y. Okamoto, A. Hansen, J. Vihinen, T. Amberla, and J. Kangastupa, "High speed, high strength microwelding of Si/glass using ps-laser pulses," Opt. Express **23**, 3427–3439 (2015).
22. I. H. W. Nordin, Y. Okamoto, I. Miyamoto, and A. Okada, "Evaluation of molten area in micro-welding of monocrystalline silicon and glass," IOP Conf. Ser. **144**, 012039 (2016).
23. I. H. W. Nordin, Y. Okamoto, A. Okada, H. Jiang, and T. Sakagawa, "Effect of wavelength and pulse duration on laser micro-welding of monocrystalline silicon and glass," Appl. Phys. A **122**, 400 (2016).
24. A. Utsumi, T. Ooie, T. Yano, and M. Katsumura, "Direct bonding of glass and metal using short pulsed laser," J. Laser Micro/Nanoeng. **2**, 133–136 (2007).
25. Y. Ozeki, T. Inoue, T. Tamaki, H. Yamaguchi, S. Onda, W. Watanabe, T. Sano, S. Nishiuchi, A. Hirose, and K. Itoh, "Direct welding between copper and glass substrates with femtosecond laser pulses," Appl. Phys. Express **1**, 82601 (2008).
26. F. Lacroix, D. Hélie, and R. Vallée, "Optical bonding reinforced by femotosecond laser welding," Proc. SPIE **8126**, 812612 (2011).
27. G. Zhang and G. Cheng, "Direct welding of glass and metal by 1 kHz femtosecond laser pulses," Appl. Opt. **54**, 8957–8961 (2015).
28. R. M. Carter, J. Chen, J. D. Shephard, R. R. Thomson, and D. P. Hand, "Picosecond laser welding of similar and dissimilar materials," Appl. Opt. **53**, 4233–4238 (2014).
29. Heraeus, "Quartz glass for optics data and properties," https://www.heraeus.com/media/media/hqs/doc_hqs/products_and_solutions_8/optics/Data_and_Properties_Optics_fused_silica_EN.pdf.
30. SCHOTT, "Optical glass data sheets," http://www.schott.com/d/advanced_optics/ac85c64c-60a0-4113-a9df-23ee1be20428/1.1/schott-optical-glass-collection-datasheets-english-17012017.pdf, p. 13.
31. Aalco metals Ltd, "Aluminum alloy 6082– T6–T651 plate datasheet," http://www.aalco.co.uk/datasheets/Aalco-Metals-Ltd_Aluminium-Alloy-6082-T6T651-Plate_148.pdf.ashx
32. J. Chen, R. M. Carter, R. R. Thomson, and D. P. Hand, "Avoiding the requirement for pre-existing optical contact during picosecond laser glass-to-glass welding," Opt. Express **23**, 18645 (2015).
33. O. P. Ciuca, R. M. Carter, P. B. Prangnell, and D. P. Hand, "Characterisation of weld zone reactions in dissimilar glass-to-aluminium pulsed picosecond laser welds," Mater. Charact. **120**, 53–62, (2016).